sustainability

MDPI

Article

Spatiotemporal Carbon Emission Characteristics and Sustainable Reduction Strategies for Road Networks: A Simulation of Targeted Road-Segment Control and Vehicle Electrification

Kun Xie [1], Peixin Guo [1], Jiayu Bao [2,*], Honghui Dong [1,*], Zhihua Xiong [1] and Chunjiao Dong [1]

[1] School of Traffic and Transportation, Beijing Jiaotong University, Shangyuancun 3, Haidian District, Beijing 100044, China; xiekun@bjtu.edu.cn (K.X.); 25120693@bjtu.edu.cn (P.G.); zhhxiong@bjtu.edu.cn (Z.X.); cjdong@bjtu.edu.cn (C.D.)

[2] Shangyu Branch of Shaoxing Public Security Bureau, No. 1117 Wangchong Road, Shangyu District, Shaoxing 312365, China

* Correspondence: 21120778@bjtu.edu.cn (J.B.); 23115116@bjtu.edu.cn (H.D.)

Abstract

Global climate change poses a critical challenge to sustainable urban development. The construction of low-carbon transportation systems is therefore a core strategy for enhancing the sustainability of mega-city road networks. Combining the characteristics of urban road traffic networks, this paper establishes a method for vehicle trip segmentation and carbon emission estimation based on GPS trajectory data (5699 vehicles, Beijing, September 2019) and the COPERT emission model, analyzing the spatiotemporal distribution characteristics of vehicle emissions. By incorporating the Life Cycle Assessment (LCA) emissions of electric vehicles, this study proposes carbon reduction strategies based on stochastic selection and ranking-based optimization from two dimensions: road-segment and vehicle electrification. Simulation methods are employed to evaluate the effectiveness of different strategies, as well as road network carbon emissions, under four vehicle electrification structures: Pyramid, Inverted Pyramid, Olive, and Dumbbell. Results indicate that carbon emission intensity rises significantly due to traffic congestion during peak hours. Under the LCA framework, Battery Electric Vehicles (BEVs) and Plug-in Hybrid Electric Vehicles (PHEVs) show significantly lower emissions than traditional Internal Combustion Engine Vehicles (ICEVs). Under the specified scenario assumptions, the ranking-based optimization scheme is estimated to yield carbon reductions approximately 2 times (segment control) and 3 times (electrification) those of the stochastic selection scheme, respectively. The study concludes that integrating EV promotion policies with precise carbon reduction control strategies can effectively mitigate urban road network carbon emissions.

Keywords: urban transportation; trajectory data; COPERT model; emission reduction strategy; sustainable mobility

Academic Editor: Marilisa Botte

Received: 23 April 2026
Revised: 29 June 2026
Accepted: 1 July 2026
Published: 3 July 2026

1. Introduction

With the escalating severity of global climate change, nations worldwide have proposed emission reduction targets. China has explicitly set the goals of achieving "Carbon Peaking" by 2030 and "Carbon Neutrality" by 2060. The transportation sector, as a major carbon emitter, requires urgent green transformation. Quantitative evidence underscores the policy urgency: Huang et al. [1] show that China's transportation sector accounts for approximately 9–10% of national CO_2 emissions, with urban road transport contributing

more than 80%. Barth and Boriboonsomsin [2] demonstrate that traffic congestion increases vehicle CO_2 emissions by 20–40% compared to free-flow conditions. Meanwhile, the Global EV Outlook 2023 [3] indicates that China's EV penetration rate surged from below 5% in 2018 to over 25% in 2022. These statistics highlight the need for targeted emission reduction strategies in urban road networks.

In recent years, progress has been made in low-carbon transportation research, particularly in emission estimation and abatement management. Liu and Zhu [4] adopted a top-down approach to estimate transport carbon emissions across 30 provinces, showing that promoting "road-to-rail" policies contributes to emission reduction. Xiao et al. [5] analyzed emission governance strategies through simulation, proposing optimizations in industrial structure, energy mix, and transport modes. Gao et al. [6] developed a mixed fleet replacement and route optimization model, finding that electrification policies help increase EV mileage. Xiao et al. [7] investigated traffic restriction policies, revealing trade-offs between ICEV reduction and increased travel costs. Liu et al. [8] combined traffic simulation with emission models to identify high-emission zones. Lv et al. [9] analyzed public transit substitutability for ride-hailing orders. Ericsson et al. [10] found that eco-friendly route choices could reduce emissions by 5–20%. Wang et al. [11] reviewed dynamic traffic assignment models for sustainable transportation. Beyond passenger travel, freight transport also contributes significantly: Lee and Stoeltje [12] developed a food assignment model showing that route-based estimation yields substantially higher emissions than Euclidean distance. Maggini et al. [13] assessed zero-carbon freight vehicles, finding fuel cell vehicles cost-competitive for medium-to-long hauls.

Despite these advances, three methodological gaps remain. (1) Road-network level: Most research relies on macro-level "top-down" approaches or single-segment emission factors, lacking fine-grained, trajectory-based spatiotemporal characterization across the entire urban road network, which makes it difficult to identify high-emission hotspots. (2) Life-cycle perspective: The emission benefits of electric vehicles are often assessed only from tailpipe emissions, without sufficient comparison of full life-cycle emissions (LCA) among BEVs, PHEVs, and ICEVs under diverse electricity mix scenarios. (3) Dual-strategy coupling: Targeted road-segment control and vehicle electrification are usually studied separately, without a coupled simulation evaluation. Moreover, most strategies rely on random selection rather than ranking-based optimization according to emission characteristics, leading to lower reduction efficiency.

To address these gaps, this study uses GPS trajectory data and the COPERT model to first analyze spatiotemporal emission characteristics of the road network, then incorporates LCA and proposes ranking-based optimization for both targeted road-segment control and vehicle electrification strategies. The specific research questions are as follows: (i) What are the spatiotemporal characteristics of vehicle carbon emissions and how does congestion affect emission intensity? (ii) Compared with stochastic selection, can ranking-based optimization (targeting the highest emitters) achieve substantially higher carbon reductions under the same intervention intensity? (iii) How do different fleet electrification structures (Pyramid, Olive, Dumbbell, Inverted Pyramid) affect network-wide carbon reduction? The marginal contribution is to provide a unified simulation framework that directly compares the reduction efficiency of stochastic versus ranking-based control strategies, using real GPS trajectory data and LCA-based electrification scenarios, and to quantify the emission reduction ratios for four fleet transition pathways.

This study therefore contributes to sustainable urban transportation by providing simulation-based evidence for ranking-oriented emission control and life-cycle-aware electrification strategies.

2. Method for Trip Segmentation and Carbon Emission Estimation Based on Trajectory Data

2.1. Trajectory Data Preprocessing and Trip Segmentation

Vehicle-mounted GPS data are frequently susceptible to factors such as signal instability and equipment malfunction, resulting in data errors and incompleteness. Consequently, data cleaning is essential to ensure the accuracy and validity of the dataset. In this study, the scikit-mobility library is employed to preprocess vehicle GPS data collected at a 30-s sampling interval, to obtain reliable and accurately traceable travel trajectories. Scikit-mobility is specifically designed for the analysis of mobility and trajectory data, supporting a diverse range of analytical tasks, including trajectory clustering, trajectory segmentation, travel pattern recognition, and trajectory prediction. The library provides two primary data structures: TrajDataFrame, primarily used for handling GPS trajectory data, and FlowDataFrame, designed for managing spatial flow data between locations. Both structures extend the standard Python Pandas DataFrame (Python version 3.12.2), facilitating the efficient processing and analysis of traffic trajectory data.

Drawing upon general database processing standards such as those described by Zheng et al. [14], and integrating the specific data field requirements of this study, the vehicle data preprocessing follows the steps outlined in Table 1.

Table 1. Travel data preprocessing.

Processing Step	Method	Description	Key Parameters
Trajectory Filtering	Scikit-mobility filtering	Filters out noise or outliers from trajectory points	Max Speed = 200 km/h
Trajectory Compression	Compression. compress	Aggregates multiple points into a single point to reduce data volume. Uses median coordinates and initial timestamp	Compression Radius = 0.05 km
Stop Detection	Stay-location detection	Detects a stop when a vehicle stays within a detection radius for a specific duration. Uses median coordinates	Detection Radius = 0.2 km Stop Duration = 10 min
Trajectory Segmentation	Trajectory splitting	Segments a daily trajectory into multiple trips based on identified stop points	--
Trajectory Validity Filtering	Trajectory validity filtering	Applies a permissive lower-bound trip screen; retained observations must also pass the speed filter, stop-detection, map-matching, and link-aggregation steps before emission estimation	Min Points = 2 Min Duration = 2 min

Table 1 reports the preprocessing thresholds used in the analysis, including the stop-duration threshold, detection radius, and minimum trip-screening criteria. These parameters define the trajectory segmentation procedure used for the subsequent emission estimation.

A sensitivity analysis on key parameters (stop duration and detection radius) was conducted as an internal check; the relative spatial patterns and strategy rankings remained stable across the tested ranges, although the absolute emission values varied moderately. These checks are not reported in detail here because they do not affect our main comparative conclusions.

In the processing of vehicle trajectory data, a temporal threshold method is commonly employed to identify stay locations and trips. This approach aggregates consecutive data points in space into a single node based on predefined criteria. Specifically, when the time

interval between data points exceeds a set threshold (e.g., 10 min), the vehicle is deemed to be at a stop, as illustrated in Figure 1. Consequently, the trajectory segment between two consecutive stops is defined as a single trip. This method effectively distinguishes between stationary and moving states, ensuring accurate data for subsequent analysis.

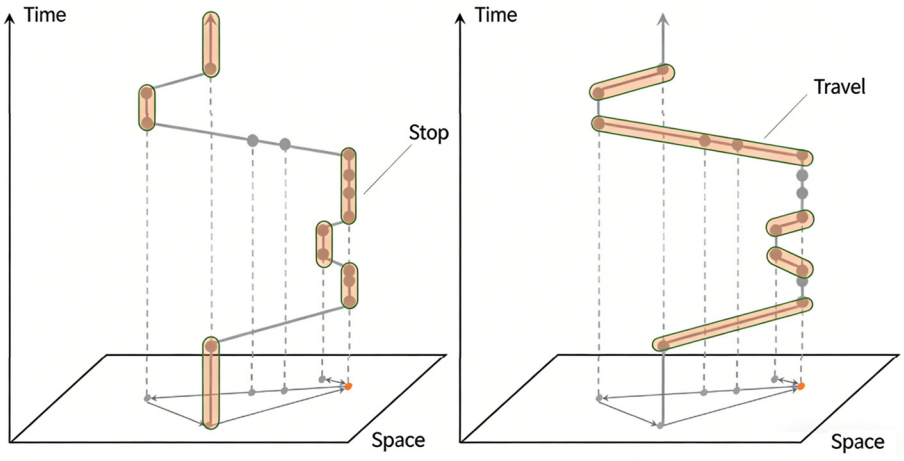

Figure 1. Travel point locus construction diagram.

The processed GPS trajectory database comprises 5699 motor vehicles. The dataset used in this study is large and complex. The raw data covers more than 40,000 vehicles, and each vehicle generates one record containing seven variables every 30 s, resulting in a very large daily data volume. Furthermore, one full week of data was used to conduct a comparative spatiotemporal analysis of carbon emissions. Extending the research period from single days to an entire week substantially increased the computational burden of data preprocessing and modelling analysis, given the already large daily data volume.

Despite the large total pool of vehicles, not all vehicles operate on roads every day. Beijing enforces a vehicle restriction policy to alleviate traffic congestion, under which each vehicle is prohibited from traveling for at least one day each week. To enhance analytical efficiency while guaranteeing reliable and unbiased comparative outcomes, we screened vehicle IDs with travel trajectories on no fewer than five days within the research week. Ultimately, 5699 vehicles were retained to examine the spatiotemporal characteristics of road network carbon emissions.

Since these selected vehicles do not travel daily, the number of active vehicles fluctuates across days, with more vehicles traveling on certain days and fewer on others. On working days, the average daily volume of trajectory records totals 2,107,100, averaging approximately 370 records per vehicle per day. On non-working days, the average daily volume is 1,524,555, averaging 268 records per vehicle per day.

For the carbon emission simulation and validation section, we further narrowed the research scope based on the 5699 qualified vehicles: the spatial boundary was focused from all 16 municipal districts to the six central urban districts of Beijing, and the temporal scope was limited to weekdays only. This filtering yielded a subset of 3390 vehicles, as summarized in Table 2. The database is structured with the Vehicle ID as the primary key and the recording timestamp as the secondary key, with trajectory sequences within the same day sorted in ascending order.

Table 2. Data Applications and Corresponding Sample Sizes.

	Temporal Scope	Spatial Scope	Sample Size
Carbon emission characteristic analysis	Workdays and non-workdays	All 16 municipal districts	5699
Carbon emission reduction strategy simulation	Workdays only	Six central districts	3390

The GPS data were collected from anonymized fleet vehicles operating in Beijing under an institutional research agreement. All vehicle identifiers were removed and replaced with random IDs. The data provider has confirmed that informed consent was obtained. The sample covers passenger cars, taxis, and light-duty freight vehicles; however, it may not fully represent all vehicle types (e.g., heavy-duty trucks). The geographical coverage includes the six central urban districts, and the sample size (5699 vehicles) is approximately 1.2% of the registered vehicles in the area. This sample is unlikely to materially affect the relative scenario comparisons, but may affect absolute emissions and transferability to other regions or fleets. Therefore, the results should be interpreted as illustrative of the methodological framework rather than as a definitive emission inventory for Beijing.

Although the sample is limited in absolute size, its aggregate speed and congestion patterns match independent navigation data. Moreover, the study focuses on relative comparisons rather than absolute emission inventories. Thus, the sample is considered adequate for the analytical purposes of this study.

2.2. Motor Vehicle Emission Estimation Model

In recent years, considerable scholarly attention has been directed towards the study of on-road motor vehicle emissions. The COPERT model has been widely adopted due to its European origins and compatibility with China's current emission standards, which allows adaptation to future regulatory changes. Multiple studies [15–18] indicate that the simulation results of the COPERT model are closer to empirical measurements compared to those of the MOBILE model. Through localization studies, Xie et al. [19] found that the emission factors calculated by the COPERT model are more consistent with real-world emission conditions. Consequently, this study selects the COPERT model to investigate the carbon emission characteristics of the road network, and the corresponding carbon emission estimation framework is outlined in Table 3.

The estimation of carbon emissions often necessitates integration with the road network environment. When calculating the total emissions of a road network, the factors considered primarily include dimensions such as vehicle travel characteristics, regional environmental attributes, and travel model attributes. These specifically include: socio-economic data [20], such as population density and GDP; road network attributes [21,22], such as road length, network density, and traffic volume; and traffic model attributes, such as travel demand models.

2.3. Method for Estimating Motor Vehicle Travel Emissions Based on COPERT

This study applies the COPERT average-speed methodology to estimate road-traffic CO_2 emissions from link-average speed and vehicle-kilometers travelled (VKT). The speed-dependent emission-factor coefficients used in the calculation are listed in Table 3. Because detailed fleet-specific information was unavailable for all sampled vehicles, the coefficients are used as an approximation for the sampled fleet, and the resulting absolute emissions should be interpreted as model-based estimates rather than a validated citywide emission inventory.

Table 3. Carbon emission measurement method diagram.

Step	Method	Schematic Diagram	Step	Method	Schematic Diagram
(1)	Vehicle trajectory construction, segmentation, and filtering		(4)	Map emission points to the nearest road-segments	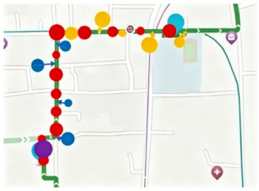
(2)	Calculate speed-dependent emissions from link-average speed and VKT		(5)	Aggregate total emissions for each road-segment	
(3)	Aggregate total emissions for each individual vehicle		(6)	Simulate different emission reduction scenarios	

The COPERT model quantifies the emissions of various pollutants by integrating key parameters such as average vehicle speed and emission factors. It also accounts for factors including fuel evaporation and mechanical wear. This provides a comprehensive emission analysis. Moreover, the model closely couples emission factors with vehicle activity data—specifically total mileage—to accurately estimate road traffic emissions. This study focuses on the application of the COPERT model in three core dimensions: exhaust emissions, fuel evaporative emissions, and tire, brake, and road surface wear.

(1) Vehicle Exhaust Emissions

Vehicle emission characteristics are significantly influenced by the engine operating state. Variations in engine operating conditions caused by different driving environments lead to substantial differences in emission levels. Consequently, when vehicles travel within an urban road network, their emissions exhibit marked heterogeneity, particularly across different road types (e.g., road-segments versus intersections).

Based on the engine operating state, vehicle emissions are categorized into two distinct phases: cold-start emissions and hot-stabilized emissions. Hot-stabilized emissions are influenced by multiple factors, including mileage (VKT), speed (dependent on road type), vehicle age, engine specifications, and vehicle weight, as expressed in Equation (1). Cold-start emissions occur during the initial phase of vehicle operation. These result in excess emissions because the engine and the catalytic converter have not yet reached their stabilized operating temperatures. They are also significantly affected by driving behavior and climatic conditions, as shown in Equation (2).

$$E_{hot;i,j,k} = N_j \times VKT_{j,k} \times e_{hot;i,j,k} \quad (1)$$

$$E_{cold;i,j} = \beta_{i,j} \times N_j \times VKT_j \times e_{hot;i,j} \times \left(e^{cold} / e^{hot} \Big|_{i,j} - 1 \right) \quad (2)$$

where, $E_{hot;i,j,k}$ represents the hot-stabilized emissions of pollutant i generated by vehicle category j traveling on road-segment k; N_j denotes the number of vehicles of category j; $VKT_{j,k}$ is the annual vehicle kilometers traveled by vehicle category j on road-segment k;

$e_{hot;i,j,k}$ denotes the hot emission factor of pollutant i for vehicle category j on road-segment k; $E_{cold;i,j}$ represent the cold-start emissions of pollutant i generated by vehicle category j; $\beta_{i,j}$ is the fraction of mileage driven with a cold engine for pollutant i and vehicle category j, which depends on the ambient temperature (t_a) and the vehicle usage pattern; VKT_j is the annual vehicle kilometers traveled by vehicle category j; $e_{hot;i,j}$ denotes the hot emission factor of pollutant i for vehicle category j; $e^{cold}/e^{hot}\Big|_{i,j}$ represents the cold/hot emission ratio for pollutant i and vehicle category j, used to quantify emissions attributed to mileage driven with a cold engine.

(2) Fuel Evaporative Emissions

Vehicle evaporative emissions primarily stem from two main sources: fuel evaporation induced by diurnal temperature fluctuations and fuel permeation losses. In simulating these emissions, the COPERT model accounts for three distinct mechanisms: diurnal emissions, running losses, and hot soak emissions. These are influenced by fuel volatility, ambient temperature, vehicle design characteristics, and driving patterns. The daily fuel evaporative emissions can be calculated using Equation (3):

$$E_{VOC} = \sum_j N_j \times \left(HS_j + e_{d,j} + RL_j\right) \quad (3)$$

where, E_{VOC} denotes the daily evaporative emissions; HS_j represents the current annual average daily hot-soak emissions for vehicle model j; $e_{d,j}$ indicates the current annual average daily emissions for vehicle model j; and RL_j signifies the current annual average daily rolling loss for vehicle model j.

(3) Wear-related Emissions

The calculation of wear-related emissions primarily incorporates tire wear, brake wear, and road surface wear generated during vehicle operation. During driving and braking deceleration, the continuous friction between the tires and the road surface causes road abrasion particles to become suspended in the atmosphere, thereby inducing severe environmental pollution issues. The specific calculation formula is presented in Equation (4):

$$TE_i = \sum_j N_j \times VKT_j \times EF_j \times f_i \quad (4)$$

where, TE_i denotes the total emissions of pollutant i resulting from road surface wear in a given area over a specified time period; EF_j represents the total emission factor for suspended particulate matter (PM) from road surface wear for vehicle type j; f_i indicates the weight ratio of PM with particle size i to the total suspended PM from road surface wear.

In calculating carbon emissions from the urban road traffic network using the COPERT model, the emission-factor parameters were derived from the COPERT methodology defined in the Guidebook [23]. The hot emission factors for gasoline passenger cars are speed-dependent and are expressed in grams per kilometer (g/km). These factors vary according to fuel type, vehicle category, and engine technology. By consolidating the speed-dependent functional relationships into a unified form, the CO_2 emission factor (EF) is expressed as Equation (5). This method encompasses emissions including Carbon Monoxide (CO), Volatile Organic Compounds (VOCs), Nitrogen Oxides (NO_x), PM, as well as Energy Consumption (EC).

$$EF = \frac{Alpha \times V^2 + Beta \times V + Gamma + Delta/V}{Epsilon \times V^2 + Zeta \times V + Eta} \times (1 - RF) \quad (5)$$

where EF denotes the speed-dependent CO_2 emission factor, expressed in g/km; V is the link-average vehicle speed, measured in km/h; Alpha, Beta, Gamma, Delta, Epsilon, Zeta, and Eta are COPERT coefficients listed in Table 4; and RF is the reduction factor.

Table 4. COPERT model parameters.

Emissions	CO_2	NO_x	VOC	EC
Alpha	5.50×10^{-12}	3.86×10^{-5}	3.55×10^{-6}	4.80×10^{-3}
Beta	-3.34×10^{-2}	-8.58×10^{-3}	-1.39×10^{-4}	-2.53×10^{-1}
Gamma	5.11×10^{0}	5.77×10^{-1}	4.74×10^{-2}	2.10×10^{1}
Delta	-1.04×10^{-7}	1.31×10^{-12}	-9.10×10^{-14}	2.54×10^{-13}
Epsilon	1.87×10^{-3}	2.70×10^{-17}	-6.44×10^{-15}	8.01×10^{-4}
Zeta	-5.29×10^{-1}	-1.31×10^{-13}	7.73×10^{-13}	9.13×10^{-2}
Eta	3.75×10^{1}	5.43×10^{0}	4.01×10^{0}	3.51×10^{0}

Given that the calculation of emissions for diverse vehicle categories necessitates a large number of equation coefficients, the parameters required by the COPERT model are presented in Table 4, with the data rounded to three significant figures.

The coefficients in Table 4 are derived from the COPERT methodology for gasoline passenger cars under typical urban driving conditions. They are used here as an approximation for the Chinese fleet; localized calibration is recommended for future studies.

We acknowledge that the current COPERT implementation relies on average speed per road-segment and does not incorporate dynamic traffic state variables such as instantaneous acceleration, deceleration, or signal delay. These factors can affect emission intensity during congested stop-and-go conditions. Future work will integrate micro-simulation models to capture such dynamics.

It should be noted that, although fuel evaporative and wear-related emission formulations are described here for completeness of the COPERT framework, the road-network CO_2 totals and carbon reduction simulations in this study are based exclusively on exhaust CO_2 emissions (Equation (5)). Evaporative and wear-related emissions are primarily associated with VOCs and particulate matter, respectively, and are therefore not included in the CO_2-focused emission estimates and reduction evaluations presented in Sections 3 and 4.

3. Analysis of Spatiotemporal Distribution Characteristics of Vehicle Carbon Emissions in Road Networks

The data were collected in 2019, representing a pre-COVID baseline. Subsequent data indicate substantial growth in both traffic volumes and electric vehicle penetration: Beijing's registered vehicle stock increased from approximately 6.346 million in 2019 to 7.589 million in 2023 and 7.882 million in 2024 [24]; national NEV ownership surged from 1.20 million in 2019 to 31.40 million by the end of 2024 [25]; and Beijing's new energy passenger vehicles reached 642,000 by 2024 [26]. The 2023 peak-hour average traffic congestion index increased by 9.67% compared with 2019 [27]. While these trends suggest that absolute emission levels may have increased, our findings should be interpreted as illustrative of the methodological framework rather than as a real-time assessment.

Since GPS data loggers can precisely record location and timestamps, travel characteristics—such as travel time and distance—can be directly derived from the GPS data. However, inferring travel modes and trip purposes requires supplementary data support, such as GIS data, respondent attributes, and intelligent algorithms [28]. Conduct-

ing characteristic analysis on the cleaned real-world data [29] facilitates the research on emission estimation.

Utilizing a database comprising 5699 motor vehicles, this study analyzes the characteristics of travel-related emissions. The statistical distribution is examined at a spatiotemporal scale defined by a 1 km grid radius and a minimum stop duration of 10 min. Key indicators investigated for each grid cell include the total number of vehicles, total VKT, average speed, and total carbon emissions. Specifically, the total number of vehicles reflects the regional travel activity level and density; total VKT embodies the intensity of travel activities within the area; average speed indicates the operational status of the road network; and total carbon emissions characterize the absolute emission level, which, when combined with total VKT, allows for the calculation of the regional carbon emission intensity. The spatial distribution of travel emissions is illustrated in Figure 2.

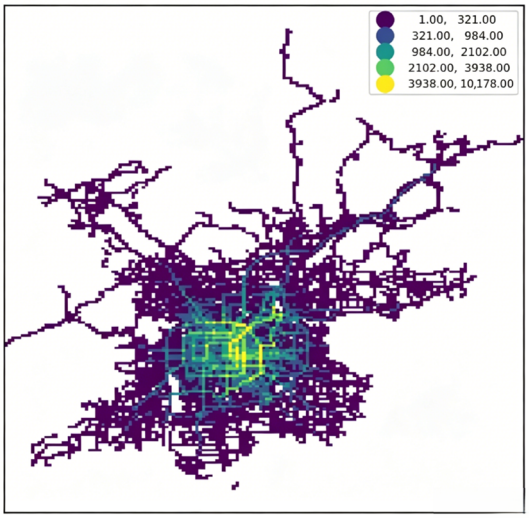

(**a**) Active vehicle counts (vehicles per 1 km grid cell)

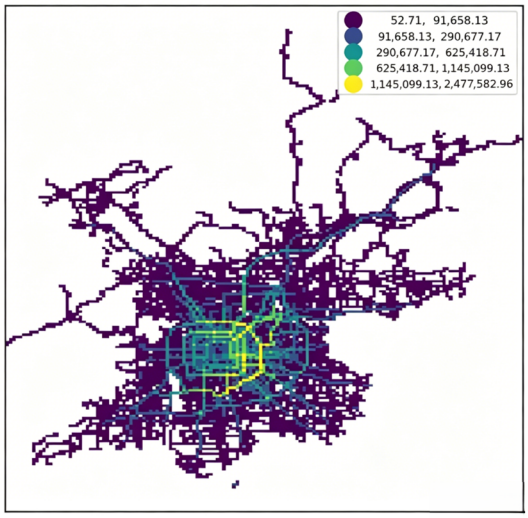

(**b**) Total VKT (VKT; km per 1 km grid cell)

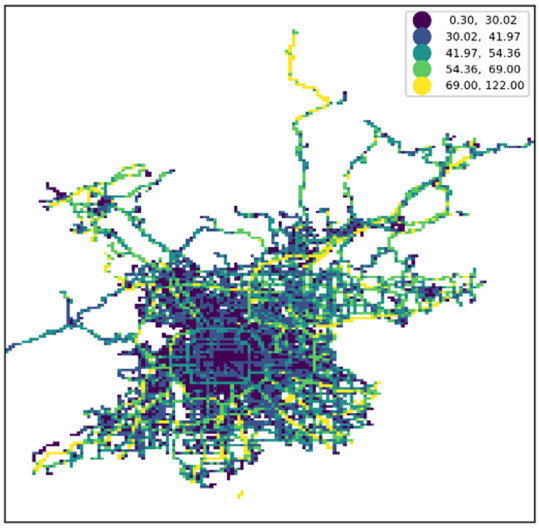

(**c**) Mean Speed (km/h)

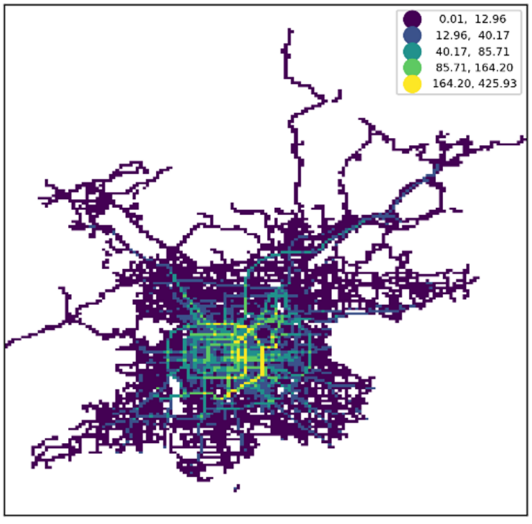

(**d**) Total CO_2 emissions (kg per 1 km grid cell)

Figure 2. Spatial distribution of daily travel emissions (1 km grid cells).

As illustrated in Figure 2, the characteristics of travel emissions align closely with the layout of the urban road network. Carbon emission features are particularly pronounced along the ring expressways and central radial arteries, spanning from the 2nd to the 6th Ring Roads. The area within the 5th Ring Road constitutes the core urban area, where both travel volume and travel distance are significantly concentrated, resulting in correspond-

ingly higher carbon emissions. Furthermore, emissions in the eastern half of the city are noticeably higher than those in the western half. Regarding road operational status, the central urban area exhibits significantly higher congestion; however, urban expressways and arterial roads are effective in enhancing the daily average travel speed. Several congestion hotspots are also observed in the peripheral areas. The overall operational status of the studied vehicles is consistent with traffic conditions reported by AutoNavi Maps. The dataset is considered suitable for relative spatial-pattern analysis, although it may not fully represent the complete urban fleet. Notably, expressways and major arterial roads (e.g., ring roads) exhibit significantly higher emission levels than collectors and local roads, consistent with their higher traffic volumes.

The scope of this research focuses on intra-day urban travel. To capture the temporal variability of the data, urban travel patterns on a representative working day (23 September 2019) and a non-working day (28 September 2019) are selected as case studies. The temporal distribution of vehicle emissions is analyzed and illustrated in Figure 3. A sampling interval of 15 min is adopted to characterize the intra-day evolution of key indicators, including the total number of vehicles, total VKT, average speed, and total carbon emissions.

Figure 3 illustrates distinct morning and evening peaks, during which operating speeds are reduced. Travel volume and intensity surge around 06:00 and 09:00, respectively, peaking at noon before a slow decline. On working days, the surge intervals are shorter and fluctuations are greater than on non-working days, with carbon emissions following a similar temporal pattern. Notably, a brief emission trough occurs during the weekday morning peak—coinciding with the lowest average speed—a pattern not observed on non-working days. To elucidate this, Figure 4 analyses the time-varying emission intensity.

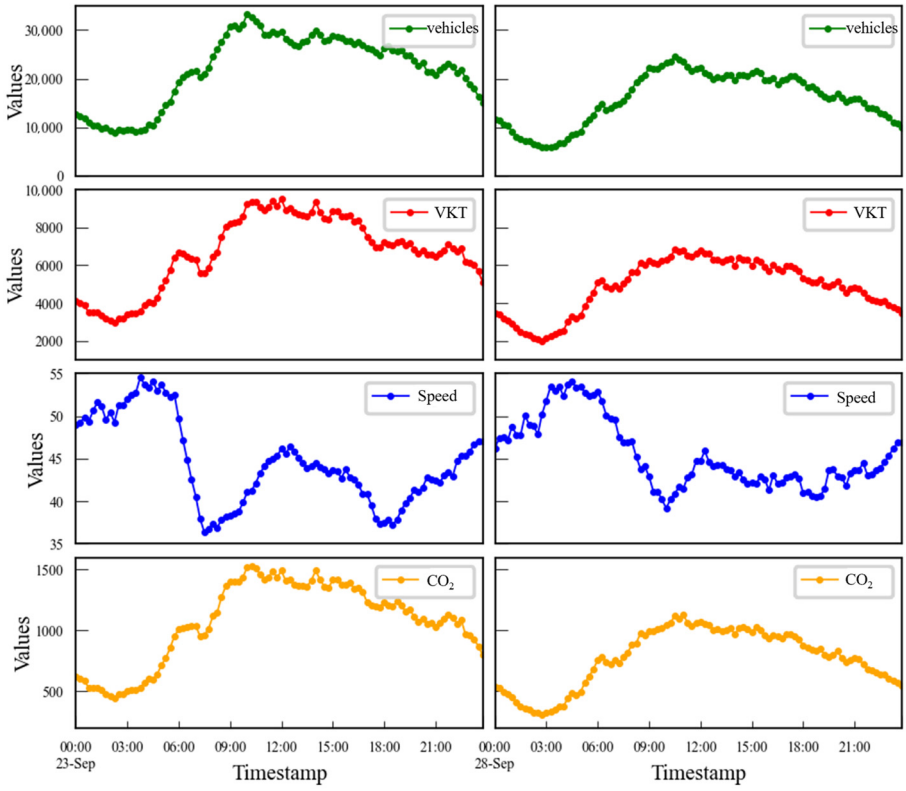

Figure 3. Temporal distribution of daily travel emissions (15-min intervals, working day vs. non-working day).

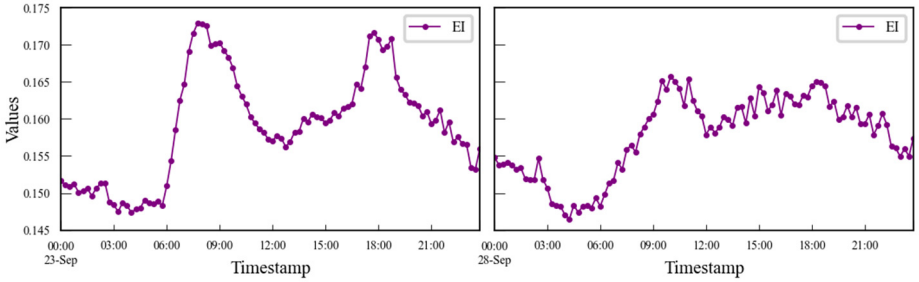

Figure 4. Temporal distribution of EI (EI is defined as CO_2 emissions per vehicle kilometer traveled (g/km), aggregated in 15-min intervals for a working day and a non-working day).

Figure 4 indicates that the degraded Level of Service (LOS) during weekday peaks significantly elevates carbon emission intensity, a pattern not observed on non-working days. Therefore, comprehensive emission analysis requires evaluating network emission intensity alongside total emissions.

The observed peak-period increase in emission intensity is consistent with lower average link speeds and the speed-dependent COPERT emission factors in Equation (5). Frequent acceleration and deceleration are possible contributing factors during congestion, but they are not explicitly represented in the present emission calculation.

The GPS sample was not weighted to match official fleet composition or origin-destination distributions. Its agreement with independent navigation data supports relative scenario comparisons, but sampling differences may affect absolute emissions and the transferability of the estimated reduction magnitudes.

Although a 1 km grid is used for macroscopic visualization (Figure 2), the subsequent emission reduction simulations and hotspot identification are based on a finer 200 m resolution grid (65,809 cells). A post-hoc grid-size check (200 m, 500 m, 1 km) suggests that the spatial pattern of high-emission cells and the relative strategy performance are broadly consistent; this internal check supports the use of the 200 m grid for the main analysis.

4. Simulation Assessment of Carbon Emission Reduction Strategies for Road Networks

4.1. Life-Cycle Emissions of EVs

Using monthly data from 2009 to 2017, previous research employed the Quantile-on-Quantile (QQ) approach and panel models to analyze the relationship between EV ownership and CO_2 emissions. Findings reveal that EVs exert a negative impact on CO_2 emissions, whereas CO_2 emissions have a weakly positive influence on EV adoption, with significant directional causality differences across countries [30]. Table A1 summarizes the relevant data derived from BP statistics [31] and the IEA Global EV Outlook 2019 [32].

For broader context, Appendix A Table A1 summarizes cross-country data on monthly CO_2 emissions and EV ownership (2009–2017). The local LCA calculations in this study (Table 5) are based on Beijing-specific parameters and 2019 fleet data, not directly on the cross-country statistics.

Propelled by supportive policies [33], China's New Energy Vehicle (NEV) fleet surged approximately 680-fold from 2013 to reach 20.41 million in 2023. In 2022 alone, sales hit 6.887 million (25.6% market share), commanding over 60% of the global market and ranking first globally. However, the comparative emission benefits of EVs and PHEVs over traditional vehicles rely heavily on the decarbonization extent of the power sector.

Table 5. Comparison of vehicles with different degrees of electrification.

CO_2 Emissions		ICEV	PHEV	BEV
Total emissions	Life Cycle Assessment (t)	33.0–35.5	33.1–34.7	26.8–29.3
	Emissions Relative to ICEVs	1.00	0.99	0.82
	Fuel Production (Gasoline and Electricity) (%)	70	63	52
Average Emissions per Kilometer	Life Cycle Assessment (g/km)	220–236	220–231	179–195
	Vehicle Manufacturing (g/km)	62–76	74–90	81–103
	Operation and Maintenance (g/km)	158–160	141–146	92–98
	Manufacturing Relative to ICEVs	1.00	1.19	1.33
	Operation and Maintenance Relative to ICEVs	1.00	0.90	0.60
	Full-life $PM_{2.5}$ (mg/km)	12.1–13.5	15.3–16.8	19.2–21.5
	Full-life SO_2 (mg/km)	8.3–9.2	10.5–11.8	13.6–15.1

Under diverse energy mix scenarios, Life Cycle Assessment (LCA) is employed to benchmark the environmental impacts of diesel and gasoline ICEVs, PHEVs, and EVs across current and future horizons [34]. The analysis assumes a 14-year service life and 150,000 km mileage, encompassing production (manufacturing, assembly, and logistics), operation, and maintenance phases. The operation phase accounts for distinct emission sources: fuel combustion for ICEVs, and non-exhaust emissions (tire, brake, and road wear) for all vehicles. While EVs eliminate direct tailpipe emissions, they shift the carbon burden upstream to the power generation sector. Calculations follow the 2006 IPCC Guidelines for National Greenhouse Gas Inventories (Equation (6)).

$$CE_i = AD_i \times NCV_i \times CC_i \times O_i \times \frac{44}{12} \times GWP \quad (6)$$

where, i denotes the fuel or energy type; CE_i represents the CO_2 emissions for energy type i, including coal, oil, natural gas, gas, etc.; AD_i is the fuel consumption; NCV_i is the conversion factor for converting raw fuel consumption into general energy units; CC_i is the average carbon content of the fuel or energy source; O_i is the carbon oxidation factor for the fuel or energy source; GWP is the global warming potential factor, with the IPCC setting a default value of 1 for carbon dioxide.

Employing the IPCC carbon emission calculation method, previous studies have compared the CO_2 emissions of EVs and ICEVs with similar mass and identical travel distances under varying energy structures. Results indicate that EV emissions are estimated to be only 37.05% of those generated by fuel-powered vehicles [35]. However, existing research results show significant discrepancies, primarily stemming from differences in vehicle models and energy mix assumptions [36].

Based on industry-average parameters for passenger vehicles, this study establishes multiple powertrain-structure scenarios to compare ICEVs, PHEVs, and BEVs from a life-cycle perspective (Table 5). The results indicate that PHEVs and BEVs have lower life-cycle CO_2, VOC, and NO_x emissions than ICEVs, whereas their $PM_{2.5}$ and SO_2 emissions are higher because of upstream electricity generation and battery manufacturing processes. Detailed numerical ranges are presented in Table 5.

As noted in Section 3, the 2019 data serve as a pre-pandemic baseline for methodological development. For a comprehensive discussion of generalization boundaries and data limitations, see Section Limitations and Practical Considerations.

4.2. Simulation Evaluation of Carbon Reduction Based on Targeted Road-Segment Emission Control

The strategies described in this section are scenario-based simulations that assume emissions on selected road-segments can be reduced by fixed percentages (e.g., 70%, 50%, 30%). They do not model actual driver rerouting behavior, DTA, congestion spillback, or network equilibrium changes. Therefore, the results should be interpreted as an upper-bound estimate of potential reductions from targeting high-emission segments. A full DTA model would be required to capture network-level interactions.

Based on the travel emission database and the road network, a carbon reduction simulation platform was developed leveraging OSMnx and skmob.tessellation. OSMnx facilitates the retrieval, modelling, and visualization of the street network, while the skmob.tessellation module executes spatial grid tessellation. Integrating GPS trajectories, vehicle carbon emissions in the six central urban districts on 23 September 2019, were quantified and assigned to individual road-segments. The resulting network structure comprises 135,665 road-segments and 65,809 grid cells with a 200 m resolution.

(1). Simulation of All-Day Carbon Emission Distribution

All-day emission data from individual travel points are aggregated. Specifically, emissions associated with the same vehicle are summed to calculate the total daily emissions per vehicle. After map matching using the Nearest Neighbor algorithm, emissions assigned to the same road link are merged to derive the total segment-level emissions. Using retrieval keys, the distinct characteristics of individual vehicles and road-segments can be identified, thereby facilitating the implementation of traffic control strategies and emission constraints.

The study area features a large-scale road network characterized by a distinct internal ring and an external ring-radial structure. While the central region exhibits high road density, it also contains several "closed zones" with no road traversal. Figure 5 illustrates the aggregated all-day carbon emissions of the road network, where brighter segments represent higher emission levels. It is evident that high-emission segments within the study scope are concentrated along ring roads and radial arteries with heavy traffic flow, which aligns with actual traffic emission patterns. Emission levels on surface roads between rings roads are relatively uniform; however, distinct "emission hotspots" caused by congestion are observable at intersections between ring roads and surface roads. In contrast, peripheral areas are characterized by lower traffic volumes and lower emission levels.

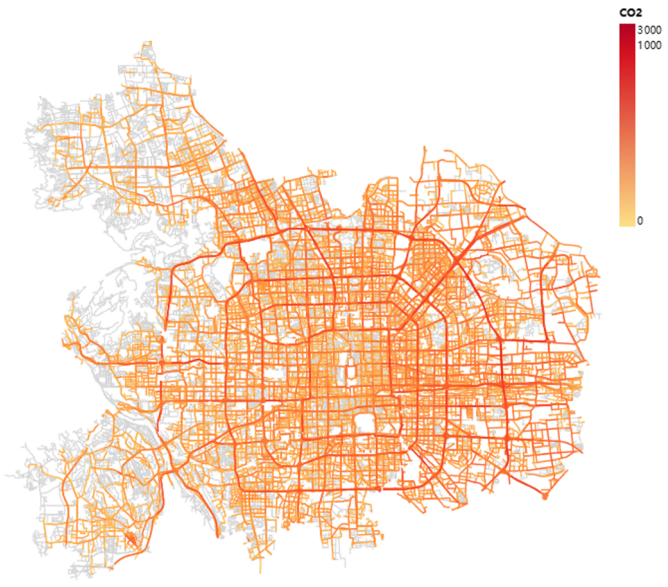

Figure 5. Spatial distribution of daily total CO_2 emissions over the road network (kg/day per road-segment).

(2). Time-Based Control and Emission Reduction Strategy

To analyze the temporal variations in carbon emissions, the periods 01:00–03:00 and 07:00–09:00 were selected as the representative off-peak and peak hours, respectively. Figure 6 illustrates the emission levels during these intervals. This comparison provides a basis for exploring differentiated control strategies based on the temporal emission distribution.

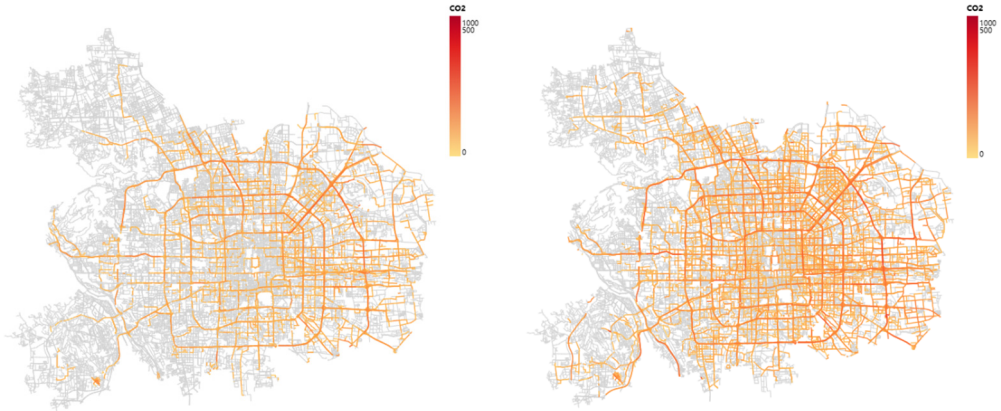

(**a**) Nighttime off-peak (01:00–03:00) (**b**) Morning peak (07:00~09:00)

Figure 6. Comparison of carbon emissions between off-peak and peak periods (two-hour intervals).

The results reveal significant temporal discrepancies in carbon emissions. In terms of total magnitude, the morning peak (07:00–09:00) involves 18,699 emitting segments generating 3454.50 kg of CO_2, averaging 0.1847 kg per segment over the two-hour interval. In contrast, the off-peak period (01:00–03:00) involves 8331 segments generating 1055.49 kg, averaging 0.1267 kg per segment. This indicates that during peak periods, not only are total network emissions significantly higher, but the average emission per segment also rises. This confirms that traffic peaks exacerbate congestion while simultaneously intensifying emission strength.

Regarding spatial distribution, off-peak emissions (01:00–03:00) are predominantly concentrated on urban expressways and arterial roads, primarily driven by night-time heavy-duty freight traffic, indicating greater spatial heterogeneity during off-peak hours. Conversely, during the morning peak (07:00–09:00), the degraded LOS on arterial roads forces traffic to divert to secondary roads (spillover effect). Consequently, high-emission segments gradually emerge between ring roads and radial arteries, leading to a network-wide increase in both congestion and emissions. This underscores the necessity for emission reduction strategies to transition from segment-based control to area-wide zonal control.

To differentiate emission characteristics by road hierarchy, we aggregated the simulation results by three functional road types: expressways, arterial roads, and collectors. As shown in Table 6, arterial roads exhibit the highest emission intensity (208.7 g/km) due to frequent congestion and stop-and-go driving during peak hours, although they do not have the highest total emissions. Expressways contribute the largest share of total daily CO_2 (42.3%) because of high traffic volumes, but their emission intensity is lower (156.2 g/km) due to higher average speeds (48.1 km/h). Collectors show the lowest total emissions and intensity, except near intersections with arterials.

Table 6. Emission Characteristics by Road Type.

Road Type	Total CO_2 Emissions (kg/day)	Share of Total (%)	Emission Intensity (g/km)	Average Speed (km/h)
Expressways	9204	42.3	156.2	48.1
Arterial roads	10,112	46.5	208.7	28.4
Collectors	2438	11.2	118.5	35.2

(3). Segment-Based Control and Emission Reduction Strategy

Currently, various measures targeting road traffic volume are available for reference, such as fuel surcharges, dedicated EV lanes, and High-Occupancy Vehicle (HOV) lanes. These measures have been proven effective in directly mitigating carbon emissions on road-segments. To achieve substantial reductions in urban carbon emissions with minimal intervention coverage, targeting high-emission segments with specific policies is likely to yield superior efficacy compared to "blind" control strategies that indiscriminately restrict irrelevant segments.

To facilitate differentiated control of road-segments, this chapter proposes two distinct strategies: the stochastic selection scheme and the ranking-based optimization scheme. The stochastic selection scheme involves randomly selecting 30% of road-segments for intervention, assuming a 50% reduction in their emissions.

Conversely, the ranking-based optimization scheme allocates reduction targets based on emission characteristics. Specifically, segments are ranked by emission levels: the top 10% of high-emission segments are assigned a 70% reduction, segments ranked 10–20% are assigned a 50% reduction, and those ranked 20–30% are assigned a 30% reduction.

This design ensures that the total number of controlled segments remains identical between the two schemes. The comparative results of these emission reduction strategies are illustrated in Figure 7, where darker blue indicates greater carbon reduction.

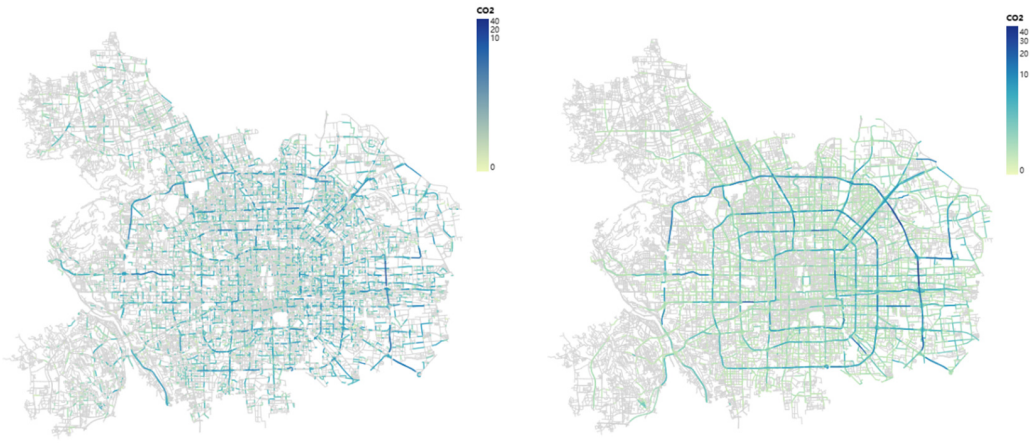

(**a**) Stochastic scheme (**b**) Optimization scheme

Figure 7. Comparison of segment-based control emission reduction schemes: stochastic selection (**a**) vs. ranking-based optimization (**b**).

The results reveal a pronounced disparity in the estimated emission reductions between the two schemes under stated fixed reduction coefficients. These values should be interpreted as scenario outputs and upper-bound potentials rather than observed effects of an implemented traffic-control or route-choice program.

In terms of total magnitude, the stochastic selection scheme targets 12,401 emitting segments and yields a total reduction of 5524.74 kg of CO_2, with an average re-

duction of 0.4455 kg per segment per day. In contrast, the ranking-based optimization scheme, which targets the same number of segments (12,401), yields a total reduction of 12,363.35 kg with an average of 0.9969 kg per segment per day. Under identical control pressure, the optimization scheme not only yields a total reduction more than twice that of the stochastic scheme but also significantly reduces the average emission per controlled segment.

Because the ranking-based scenario, by design, assigns the largest assumed reductions to the highest-emitting segments, it concentrates the estimated benefits on ring roads and radial arterials. The comparison quantifies the potential gain from targeted allocation under equal intervention coverage; it does not independently verify a causal policy effect.

In terms of segment structure, the ranking-based scheme concentrates its reductions on critical urban emission segments, including links with high emissions along ring roads and radial arteries. The ranking optimization scheme is therefore estimated to concentrate its estimated reductions on the highest-emission links, including ring roads and radial arterials, thereby targeting the main 'emission hotspots' within the urban road network. Collectively, these findings indicate a higher potential reduction for the ranking-based allocation rule under the assumed scenario conditions.

The spatial pattern of reduction differs between the two schemes: the stochastic scheme reduces emissions diffusely, whereas the ranking scheme concentrates reductions on the highest-emission segments (mainly ring roads and radial arteries). This highlights the importance of spatially targeted interventions.

The superior efficiency of the ranking-based scheme stems from the highly skewed emission distribution: in our dataset, the top 10% of vehicles contribute 34.7% of total CO_2, and the top 10% of road-segments contribute 28.2%. Concentrating interventions on these high-emitting units therefore yields disproportionately large reduction per controlled unit.

The superior efficiency of the ranking-based scheme aligns with the sustainability principle of achieving greater environmental benefits without increasing intervention scale or social disruption.

4.3. Simulation Evaluation of Carbon Reduction Considering Vehicle Electrification

The cleaned GPS database contains 5699 unique anonymized vehicles. The working-day scenario analyzed in this study uses 3390 vehicles observed on 23 September 2019; therefore, the 10% vehicle-replacement comparison includes 339 vehicles. This 339-vehicle set is derived from the observed working-day sample and should not be interpreted as a subsample of the 41,338-vehicle fleet-structure scenario. The 41,338-vehicle value is used only as an assumed scenario size for the fleet-composition analysis, rather than as a validated expansion of the sampled vehicles to the registered vehicle population.

Current research increasingly prioritizes operational emission control, with vehicle electrification emerging as a widely adopted abatement strategy. Premised on "zero tailpipe emissions" during operation, this measure significantly reduces network-wide carbon levels. Furthermore, compared with indiscriminate controls such as license plate rationing, policies targeting the electrification of high-emission vehicles demonstrate superior reduction efficacy.

To investigate the efficacy of differentiated vehicle electrification strategies, this study designs two scenarios: a stochastic selection scheme and a ranking-based optimization scheme. The stochastic scheme randomly selects 10% of the fleet for electrification, whereas the optimization scheme targets the top 10% of highest-emitting vehicles based on emission characteristics. Compared with emission characteristics on non-working days, carbon mitigation on working days is of higher practical significance. Therefore, a subsample of 3390 vehicles on 23 September 2019 (a working day) was selected for simulation assessment.

Both schemes assume zero operating emissions for electrified units at the same penetration rate. Here, "zero operating emissions" refers only to tailpipe CO_2. Upstream emissions from electricity generation are accounted for in the life-cycle assessment (LCA) values used in Table 5. Therefore, the net emission reduction in the electrification scenarios reflects well-to-wheel effects, not merely tailpipe savings. Figure 8 illustrates the comparative reduction effects, where darker blue indicates greater emission reduction.

(**a**) Stochastic scheme (**b**) Optimization scheme

Figure 8. Comparison of vehicle electrification emission reduction schemes: stochastic selection (**a**) vs. ranking-based optimization (**b**).

Figure 8 shows a pronounced difference in the estimated emission reductions between the two vehicle-replacement scenarios. The stochastic scheme, involving the replacement of 339 vehicles, yields an estimated cumulative tailpipe CO_2 reduction of 4308.16 kg, with an average of 12.71 kg per vehicle per day. Under the same 10% replacement rate, the ranking-based selection scheme is estimated to produce a cumulative reduction of 12,920.51 kg and an average of 38.11 kg per vehicle per day, approximately three times that of the stochastic scheme, reflecting that the ranking-based scenario prioritizes the highest-emitting vehicles. Spatially, compared with stochastic selection, the ranking-based scenario concentrates the estimated reductions along high-emission expressways and arterial roads, with additional reductions on secondary roads in the central district. These results should be interpreted as tailpipe-only upper-bound scenario outputs rather than observed effects of an implemented electrification policy.

Figure 9 contrasts the total network emission reductions of the stochastic scheme and the ranking-based optimization scheme across varying electrification penetration rates. The stochastic scheme exhibits an approximately linear growth relationship between reduction magnitude and penetration rate. In contrast, the ranking-based scheme shows a more complex variation pattern. Accordingly, following existing research [37], this paper employs the Generalized Logistic Function (GLF) to fit the data via the least squares method, as expressed in Equation (7).

$$f(x) = \frac{\alpha}{(1 + \beta \cdot e^{-\gamma x})^{\frac{1}{v}}} \tag{7}$$

where, α represents the upper asymptote, β denotes the growth range, γ signifies the growth rate, and v indicates the slope of the curve.

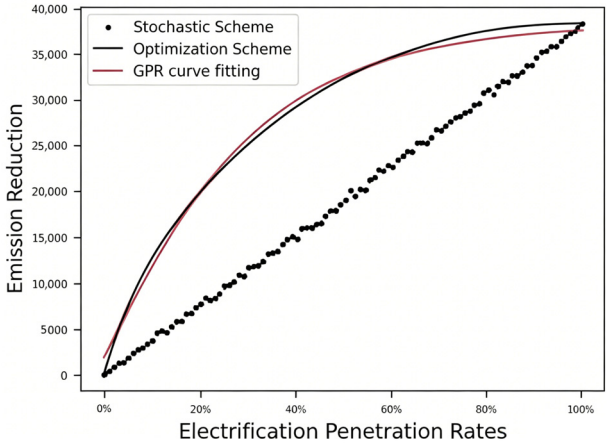

Figure 9. Comparison of total CO_2 reduction under different electrification penetration rates for stochastic and ranking-based schemes.

The negative values of β and v are a result of the specific parameterization of the GLF used here; they do not indicate negative growth but rather a decreasing rate of increase after the inflection point. Residual diagnostics confirm no systematic bias.

Figure 9 illustrates the curve fitting results for the ranking optimization scheme. The model achieves a high goodness of fit with an R^2 of 0.9956. Specific fitted parameters include a growth range β of -0.9036, a growth rate γ of 4.1244, and a curve slope v of -0.7874.

To examine how the choice of ranking factor affects the estimated reduction potential, Figure 10 compares sequential emission reductions for road-segment control and vehicle-replacement scenarios when intervention units are prioritized by different ranking factors. Most ranking factors show similar diminishing-return patterns, suggesting rapid increases when the highest-ranked units are controlled first, followed by gradual levelling-off as the control ratio increases. The acceleration-based curve differs from the other factors because acceleration is a signed and highly variable indicator. In this analysis, acceleration is used only as an exploratory ranking variable and is not an input to the COPERT emission calculation.

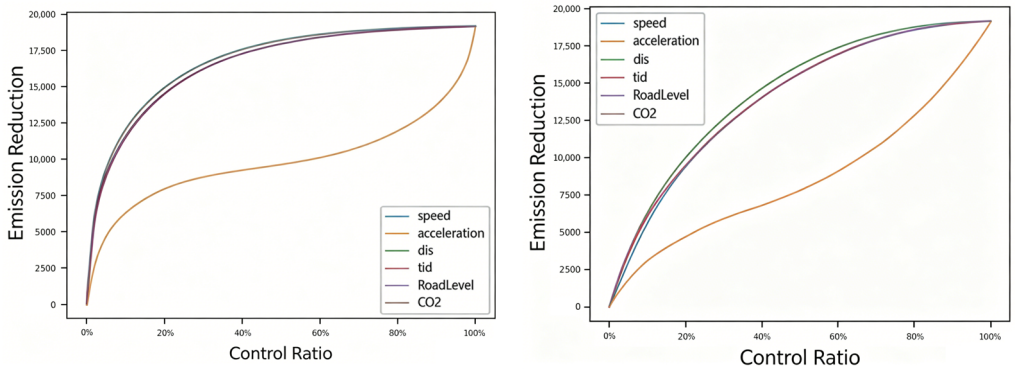

(**a**) Road-segment control (**b**) Vehicle electrification

Figure 10. Comparison of emission reduction effects for different control factors.

Subsequently, the analysis incorporates the Life Cycle Assessment (LCA) emission-intensity ranges of ICEVs, PHEVs, and BEVs to evaluate LCA-adjusted fleet-composition scenarios. To compare different electrification pathways on a common analytical basis, an assumed fleet size of 41,338 vehicles is used for the scenario analysis. Figure 11 illustrates the estimated emission reductions under four assumed fleet-composition structures: Pyramid, Olive, Dumbbell, and Inverted Pyramid.

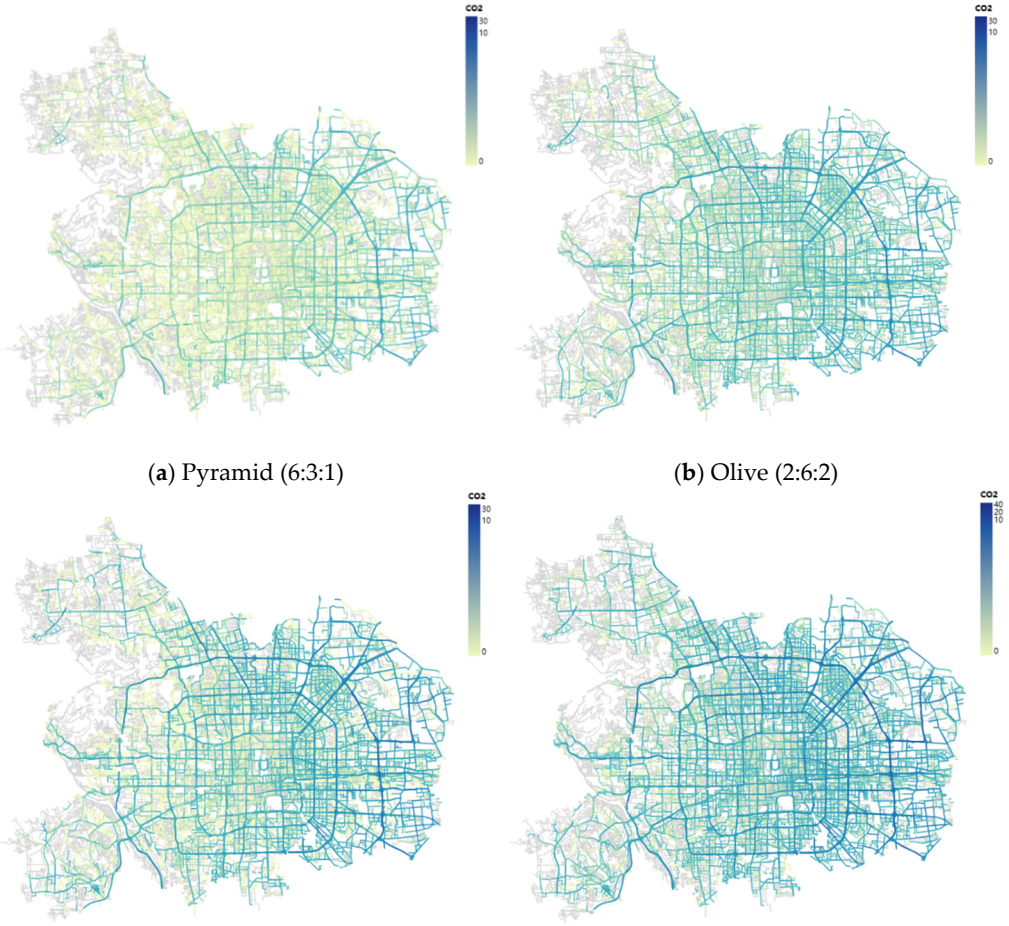

(**a**) Pyramid (6:3:1) (**b**) Olive (2:6:2)

(**c**) Dumbbell (4:2:4) (**d**) Inverted Pyramid (1:3:6)

Figure 11. Comparison of emission reduction effects across four fleet electrification structures (ICEV:PHEV:BEV ratios) under LCA accounting.

The reported reduction factors and the approximate 1:5:10:30 ratio should therefore be interpreted within the stated scenario assumptions; further sensitivity analyses using alternative thresholds and random seeds would be needed to assess their robustness.

The Pyramid structure corresponds to the nascent stage of electrification where fossil fuel vehicles predominate, while the Inverted Pyramid represents a mature stage where EVs far outnumber internal combustion units. Both the Olive and Dumbbell structures depict transitional phases under distinct strategic orientations. Specifically, the Olive structure emphasizes the promotion of hybrid electric vehicles (HEVs) to significantly reduce the fossil fuel share without pursuing full electrification immediately. Conversely, the Dumbbell structure adopts a dual-track strategy by actively promoting Battery Electric Vehicles while retaining a substantial number of fuel vehicles, allowing both to coexist as major market components.

Simulation results based on a fleet of 41,338 vehicles indicate that the Pyramid structure yields an emission reduction of 61.80 kg, the Olive structure 304.19 kg, the Dumbbell structure 683.88 kg, and the Inverted Pyramid structure 1771.92 kg. These findings suggest that the carbon reduction potentials of the four structures follow an approximate ratio of 1:5:10:30.

The emission reduction differences among the four fleet structures are driven by two mechanisms: (i) the life-cycle CO_2 per km of each powertrain (BEV < PHEV < ICEV, as shown in Table 5), and (ii) the proportion of high-emitting ICEVs replaced. The Inverted Pyramid achieves the largest reduction by maximizing BEV share, but requires substantial

grid decarbonization and charging infrastructure. The Olive structure offers moderate gains with lower upfront investment, while the Dumbbell structure provides a balanced transition. Policymakers can select a pathway based on local conditions: regions with clean electricity should prioritize BEV-dominant structures (Inverted Pyramid); regions with limited grid capacity may favor PHEV-heavy pathways (Olive).

The above electrification analysis assumes uniform grid emission factors and perfect charging accessibility. In reality, China's power grid exhibits significant spatial heterogeneity (e.g., northern coal-dominated grids vs. southwestern hydro-rich grids). Additionally, uneven charging station distribution may constrain EV usage in certain areas. To bound the impact, we conducted a sensitivity analysis: using regional emission factors for Beijing (385 g CO_2/kWh) vs. the national average (550 g CO_2/kWh), the carbon reduction of BEVs improves by 28%. Conversely, in coal-heavy regions (e.g., Shanxi, 780 g CO_2/kWh), BEV life-cycle emissions approach those of HEVs. Therefore, the reduction ratios reported (1:5:10:30) apply to grids with moderate decarbonization. Future work should integrate spatially explicit grid emission factors and charging station locations.

Furthermore, the vehicle electrification analysis does not account for regional variations in power generation mix or charging infrastructure accessibility, which may affect real-world emission reduction efficacy. Future studies should incorporate time-dependent and location-specific grid emission factors.

5. Conclusions

Integrating trajectory data with vehicle trip segmentation, this paper establishes a COPERT-based method to analyze the spatiotemporal characteristics of road-network CO_2 emissions. The study further evaluates targeted road-segment emission-control and vehicle-replacement scenarios, and incorporates Life Cycle Assessment (LCA) emission-intensity ranges to compare fleet-composition scenarios involving ICEVs, PHEVs, and BEVs. The results are interpreted as model-based scenario estimates rather than observed effects of implemented traffic-control or electrification policies. The main conclusions are as follows:

(1) Carbon emissions in the sampled trajectories are concentrated in central urban areas, major ring roads, and radial arterials, with higher emission levels observed during peak periods. The increase in morning-peak emission intensity is consistent with lower link-average speeds and the speed-dependent COPERT emission factors, indicating that emission-intensity should be considered alongside total emissions when identifying road-network hotspots. The LCA comparison, based on the applied emission-intensity ranges, indicates that BEVs and PHEVs have lower life-cycle CO_2, VOC, and NO_x emissions than ICEVs, but higher $PM_{2.5}$ and SO_2 emissions because of upstream electricity generation and battery manufacturing processes.

(2) Simulation assessments of targeted road-segment emission-control scenarios indicate that the ranking-based scheme assigns tiered reduction coefficients according to segment-level emission rankings. Specifically, the scheme assumes emission reductions of 70%, 50%, and 30% for the top, second, and third deciles of high-emission segments, respectively, whereas the stochastic selection scheme applies a uniform 50% reduction to a randomly selected 30% of segments. Under these stated assumptions and equal coverage, the ranking-based scheme yields an estimated total CO_2 reduction over twice that of the stochastic selection scheme. This comparison quantifies the potential gain from targeted allocation to high-emission segments, but it should not be interpreted as independent evidence of an implemented route-choice or traffic-control effect.

(3) Simulation assessments of vehicle-replacement scenarios indicate that the ranking-based scheme, which targets the top 10% highest-emitting vehicles in the observed

working-day sample, produces an estimated tailpipe-only CO_2 reduction approximately three times that of the stochastic selection scheme under the same 10% replacement rate. Spatially, the ranking-based scheme covers high-emission expressways and arterial roads more extensively than the stochastic scheme and also includes secondary roads in the central district. These results suggest a broader spatial distribution of estimated reductions under the assumed replacement scenario, but they should be interpreted as upper-bound scenario outputs under a zero-tailpipe-emission assumption rather than as observed effects of an implemented electrification policy.

(4) For the illustrative 41,338 vehicle fleet composition scenario, the Pyramid, Olive, Dumbbell, and Inverted Pyramid electrification structures yield emission reductions of 61.80 kg, 304.19 kg, 683.88 kg, and 1771.92 kg, respectively. These results indicate that the carbon reduction potentials of the four structural types follow an approximate ratio of 1:5:10:30.

The reported reduction ratios are derived from simulation scenarios with simplified assumptions: fixed emission reduction percentages for controlled segments, zero tailpipe emissions for EVs (while upstream emissions are included via LCA), and no modelling of behavioral rerouting or network equilibrium. Practical implementation of these strategies would require considering cost-effectiveness, charging infrastructure availability, driver compliance, and potential rebound effects. Future research should integrate DTA and real-world EV deployment data to validate these findings.

From a policy perspective, the key decision-oriented metrics derived from our simulation results are as follows:

Controlling the top 10% of highest-emitting road-segments (ranking-based optimization scheme, with tiered reductions of 70%/50%/30% for the 0–10%, 10–20%, and 20–30% segments respectively) achieves a daily CO_2 reduction of 12,363 kg, which is 2.24 times that of randomly controlling the same number of segments (5525 kg).

For vehicle electrification, targeting the top 10% highest-emitting vehicles for replacement (ranking-based scheme) yields a daily reduction of 12,921 kg under a 10% electrification rate, which is 3 times that of random selection (4308 kg). As the electrification rate increases, the cumulative reduction follows a generalized logistic growth curve (Figure 9). Under full Life Cycle Assessment (LCA) accounting, different fleet transition pathways (Pyramid → Olive → Dumbbell → Inverted Pyramid) provide stepwise reduction potentials in an approximate ratio of 1:5:10:30, corresponding to daily reductions of 61.80 kg, 304.19 kg, 683.88 kg, and 1771.92 kg, respectively, for the studied fleet of 41,338 vehicles.

These metrics directly support policy decisions on targeted road network control (prioritizing top-emitting segments) and phased electrification strategies (prioritizing high-emitting vehicles and transitioning through the four fleet structures).

Limitations and Practical Considerations

These findings are based on a specific dataset (5699 vehicles, 2019, one mega-city) and the COPERT + LCA framework. Generalization to other networks requires attention to the following boundaries:

Model applicability: The absolute emission values and reduction ratios may vary with fleet composition, renewable energy share, and driving cycles. However, the relative superiority of ranking-based strategies is expected to hold wherever emissions follow a skewed (Pareto-like) distribution, common in urban traffic.

Targeted road-segment emission control implementation: The ranking-based strategy needs real-time identification of high-emission segments and dynamic route recommen-

dations (e.g., via navigation apps). Where such infrastructure is absent, static signs or time-based restrictions can approximate it, albeit with reduced effectiveness.

Electrification implementation: Identifying high-emitting vehicles requires periodic testing or onboard diagnostics. Policy tools include progressive scrappage subsidies, emission-differentiated charges, or low-emission zones. Among fleet structures, the Inverted Pyramid (BEV-dominant) offers the largest reduction but demands high upfront investment in charging and grid upgrades; the Olive structure (PHEV-heavy) incurs lower costs but yields only moderate reductions.

Collaborative strategies: Joint application of targeted road-segment emission control and electrification was not explicitly simulated. Their combined effect could be complementary and should be tested in future work (e.g., using integrated simulation models that capture both rerouting behavior and fleet composition changes). A practical pathway for future investigation might include the following: (1) deploying ranking-based guidance via existing navigation apps; (2) phasing in electrification starting with top 10% high-emitters using targeted subsidies; (3) gradually shifting from Pyramid to Inverted Pyramid as infrastructure matures. However, the actual synergy remains to be quantified.

In summary, the empirical support for the ranking-based strategies and the 1:5:10:30 ratio holds for the studied network. Transferring insights to other cities requires local recalibration. The primary contribution is a methodological framework and relative performance benchmarks, not absolute predictions.

From a sustainability perspective, this study provides four key contributions: (i) a data-driven framework to quantify the spatiotemporal heterogeneity of road network carbon emissions, enabling targeted interventions with minimal social cost; (ii) a direct comparison of stochastic versus ranking-based strategies, demonstrating that the latter achieves 2–3 times higher carbon reduction per controlled unit, thereby improving resource efficiency—a core sustainability principle; (iii) life-cycle assessment (LCA)-based electrification scenarios that reveal trade-offs (lower CO_2 but higher $PM_{2.5}$ and SO_2), guiding balanced sustainable policy design; (iv) a clear ordering of four fleet transition pathways (Pyramid → Olive → Dumbbell → Inverted Pyramid) with reduction ratios of 1:5:10:30, enabling phased, cost-effective sustainability targets for urban transport systems.

Author Contributions: K.X.: Formal analysis, Methodology, Software, Investigation, Data curation, Writing—original draft. P.G.: Data curation, Writing—review & editing. J.B.: Conceptualization, Resources, Writing—review & editing, Visualization, Supervision. H.D.: Conceptualization, Resources, Writing—review & editing, Visualization, Supervision. Z.X.: Data curation, Writing—review & editing. C.D.: Data curation, Writing—review & editing. All authors have read and agreed to the published version of the manuscript.

Funding: This work was supported by the Major Program of National Social Science Foundation (Grant number: 23&ZD138).

Institutional Review Board Statement: Not applicable.

Informed Consent Statement: Not applicable.

Data Availability Statement: The data presented in this study are available on request from the corresponding author due to restrictions imposed by the project confidentiality agreement and personal privacy protection regulations, and therefore are not publicly available. The core dataset consists of real vehicle GPS trajectory data, which contains sensitive personal travel information and confidential project data resources.

Conflicts of Interest: The authors declare no conflicts of interest.

Abbreviations

The following abbreviations are used in this manuscript:

BEV	Battery Electric Vehicle
CO_2	Carbon dioxide
COPERT	Computer Programme to calculate Emissions from Road Transport
DTA	Dynamic Traffic Assignment
EC	Energy Consumption
EV	Electric Vehicle
FCEV	Fuel Cell Electric Vehicle
GDP	Gross Domestic Product
GIS	Geographic Information System
GLF	Generalized Logistic Function
GPS	Global Positioning System
GWP	Global Warming Potential
HOV	High-Occupancy Vehicle
ICEV	Internal Combustion Engine Vehicle
IEA	International Energy Agency
IPCC	Intergovernmental Panel on Climate Change
LCA	Life Cycle Assessment
LOS	Level of Service
NEV	New Energy Vehicle
NO_x	Nitrogen Oxides
PHEV	Plug-in Hybrid Electric Vehicle
PM	Particulate Matter
QQ	Quantile-on-Quantile
VKT	Vehicle Kilometers Traveled
VOC	Volatile Organic Compounds

Appendix A

Table A1. Monthly CO_2 emissions (million tonnes) and EV ownership (thousands) by country.

Country	Variable	Mean	Standard Deviation	25th Percentile	50th Percentile	75th Percentile	Mini	Max
China	CO_2	8548.26	801.42	7680.70	8966.30	9204.20	7214.80	9232.60
	EV	261.46	421.81	6.98	32.22	312.77	0.48	1227.77
France	CO_2	338.16	24.31	314.80	337.70	361.50	304.20	371.20
	EV	24.65	38.38	0.01	3.03	31.54	0.01	118.77
Germany	CO_2	773.05	21.31	753.50	765.40	795.10	749.40	807.20
	EV	21.17	34.86	0.09	1.89	24.93	0.02	109.56
India	CO_2	2130.30	1047.04	1594.40	1850.50	2251.00	1365.50	5146.30
	EV	2.81	2.10	0.88	2.86	4.35	0.37	6.80
Japan	CO_2	1215.38	54.86	1180.50	1196.90	1273.10	1110.70	1284.50
	EV	79.50	71.79	16.14	69.46	126.40	1.08	205.35
Netherlands	CO_2	218.14	11.58	209.10	216.30	231.20	199.70	234.10
	EV	39.91	48.64	0.27	17.47	87.53	0.01	119.33
Norway	CO_2	36.37	0.74	35.90	36.50	36.80	35.20	37.50
	EV	38.35	58.53	0.40	7.15	69.17	0.01	176.31
UK	CO_2	488.46	57.01	435.70	497.40	529.00	398.20	568.40
	EV	24.35	41.53	1.22	2.89	24.08	0.22	133.67
Cross-country Pooled Statistics	CO_2	1718.52	2709.15	269.15	658.90	1325.00	35.20	9232.60
	EV	54.89	152.90	0.54	5.43	51.50	0.01	1227.77

References

1. Huang, Z.; Ji, L.; Yin, J.; Chen, L.; Wang, J.; Yin, H.; Ding, Y.; Cai, B.; Yan, G. Peak Pathway of China's Road Traffic Carbon Emissions. *Res. Environ. Sci.* **2022**, *35*, 385–393. [CrossRef]
2. Barth, M.; Boriboonsomsin, K. Real-World Carbon Dioxide Impacts of Traffic Congestion. *Transp. Res. Rec.* **2008**, *2058*, 163–171. [CrossRef]
3. IEA. *Global EV Outlook 2023*; International Energy Agency: Paris, France, 2023. Available online: https://www.iea.org/reports/global-ev-outlook-2023 (accessed on 26 April 2023).
4. Liu, Z.; Chu, L. Effects of carbon emission reduction from freight structure adjustment at provincial level in China. *J. Transp. Syst. Eng. Inf. Technol.* **2024**, *24*, 24–33. [CrossRef]
5. Xiao, H.; Deng, Z.; Ren, Y.; Ren, X. Urban transportation carbon emission prediction model and carbon reduction strategies. *J. Chongqing Jiaotong Univ. (Nat. Sci.)* **2023**, *42*, 85–92+98.
6. Gao, Y.; Qiao, Y.; Xu, M. Effects analyses of delivery fleet renewal policies considering electric vehicle deployment and routing optimization. *Chin. J. Manag. Sci.* **2025**, *33*, 156–165. [CrossRef]
7. Xiao, J.; Wang, C.; Chen, P.; Niu, Y. The multi-energy heterogeneous fleet vehicle routing optimization under urban traffic restriction. *Syst. Eng. Theory Pract.* **2017**, *37*, 1339–1348. [CrossRef]
8. Liu, B.; Lin, J.; Liu, Y.; Zhang, D. Optimization of urban traffic microsimulation model for carbon emission reduction. *J. Syst. Simul.* **2024**, *36*, 859–872. [CrossRef]
9. Lv, Y.; He, L.; Sun, H.; Xu, G. Substituted relationship between ride-hailing and public transit and emission reduction potential. *J. Transp. Syst. Eng. Inf. Technol.* **2023**, *23*, 11–23. [CrossRef]
10. Ericsson, E.; Larsson, H.; Brundellfreij, K. Optimizing route choice for lowest fuel consumption—Potential effects of a new driver support tool. *Transp. Res. Part C Emerg. Technol.* **2006**, *14*, 369–383. [CrossRef]
11. Wang, Y.; Szeto, W.Y.; Han, K.; Friesz, T.L. Dynamic traffic assignment: A review of the methodological advances for environmentally sustainable road transportation applications. *Transp. Res. Part B Methodol.* **2018**, *111*, 370–394. [CrossRef]
12. Lee, E.H.; Stoeltje, G. How far does your food travel on the highway? Food miles and carbon footprint. *J. Clean. Prod.* **2025**, *518*, 145915. [CrossRef]
13. Maggini, M.; Loreti, G.; Santoni, F.; Facci, A.L.; Ubertini, S.; Cigolotti, V.; Monteleone, G. Technical assessment and economic analysis of zero-carbon freight road transportation vehicles. *Int. J. Hydrogen Energy* **2026**, *212*, 153707. [CrossRef]
14. Zheng, Y. Trajectory Data Mining: An Overview. *ACM Trans. Intell. Syst. Technol.* **2015**, *6*, 1–41. [CrossRef]
15. Ma, Y.; Liu, Q.; Lei, G.; LI, T.; Luan, S. Application of Vehicular Emission Models and Comparison of Their Adaptability. *Acta Sci. Nat. Univ. Pekin.* **2008**, *44*, 308–316. [CrossRef]
16. Cheng, Y.; Yu, L.; Wang, H.; Hao, Y.; Song, G. Comparative study of MOBILE and COPERT emission models based on PEMS. *J. Transp. Syst. Eng. Inf. Technol.* **2011**, *11*, 176–181. [CrossRef]
17. Wang, H.; Fu, L.; Zhou, Y.; Du, X.; Ge, W. Trends in vehicular emissions in China's mega cities from 1995 to 2005. *Environ. Pollut.* **2010**, *158*, 394–400. [CrossRef] [PubMed]
18. Sun, D.; Zhang, K.; Shen, S. Analyzing spatiotemporal traffic line source emissions based on massive didi online car-hailing service data. *Transp. Res. Part D Transp. Environ.* **2018**, *62*, 699–714. [CrossRef]
19. Xie, S.; Song, X.; Shen, X. Calculating Vehicular Emission Factors with COPERT III Mode in China. *Environ. Sci.* **2006**, *27*, 415–419. [CrossRef]
20. Cai, H.; Xie, S. Estimation of vehicular emission inventories in China from 1980 to 2005. *Atmos. Environ.* **2007**, *41*, 8963–8979. [CrossRef]
21. Zheng, J.; Che, W.; Wang, Z. Traffic flow and road network-based spatial allocation of regional mobile source emission inventories. *Acta Sci. Circumstantiae* **2009**, *29*, 815–821. [CrossRef]
22. Lindhjem, C.E.; Pollack, A.K.; Denbleyker, A.; Shaw, S.L. Effects of improved spatial and temporal modeling of on-road vehicle emissions. *J. Air Waste Manag. Assoc.* **2012**, *62*, 471–484. [CrossRef] [PubMed]
23. European Environment Agency. *EMEP/EEA Air Pollutant Emission Inventory Guidebook 2023*; European Environment Agency: Copenhagen, Denmark, 2023; p. 18. Available online: https://www.eea.europa.eu/publications/emep-eea-guidebook-2023 (accessed on 2 October 2023).
24. Data Issuance. Available online: https://jtgl.beijing.gov.cn/jgj/jgxx/ywsj/index.html (accessed on 30 June 2026).
25. The Total Number of NEV in China Has Exceeded the 30 Million Mark, Embarking on a Fast Track of Rapid Development. Available online: https://nev.ofweek.com/2025-01/ART-71008-8120-30656223.html (accessed on 27 January 2025).
26. What is the Vehicle Usage Situation in Beijing? Available online: https://www.pcauto.com.cn/wd/4369532.html (accessed on 19 June 2025).
27. Where Has the "Congestion Index" Gone on the Official Website of Beijing Municipal Commission of Transport? The Official Response: It Is Under Upgrade. Available online: https://www.ximalaya.com/sound/781667855 (accessed on 6 December 2024).

28. Bohte, W.; Maat, K. Deriving and validating trip purposes and travel modes for multi-day GPS-based travel surveys: A large-scale application in the Netherlands. *Transp. Res. Part C Emerg. Technol.* **2009**, *17*, 285–297. [CrossRef]
29. Lin, X.; Zhang, Y.; Luo, Z.; Lin, P.; Lin, L.; Yao, K.; Li, M.; Wen, H. Study on measuring method of vehicle carbon emission in expressway network. *J. South China Univ. Technol. (Nat. Sci. Ed.)* **2002**, *50*, 22–28. [CrossRef]
30. Xu, B.; Sharif, A.; Shahbaz, M.; Dong, K. Have electric vehicles effectively addressed CO_2 emissions? Analysis of eight leading countries using quantile-on-quantile regression approach. *Sustain. Prod. Consum.* **2021**, *27*, 1205–1214. [CrossRef]
31. BP. *Growing the Business and Advancing the Energy Transition*, 67th ed.; BP: London, UK, 2018. Available online: https://www.bp.com/api/files/6cqieuqhq4no/master/1FhAMNbetMqbWhRPL5LMh3/108d032f63dad4ac0cdacac990ca9833/bp-annual-report-and-form-20f-2018.pdf (accessed on 29 March 2019).
32. International Energy Agency. *Global EV Outlook 2019: Scaling-Up the Transition to Electric Mobility [M/OL]*; OECD: Paris, France, 2019. Available online: https://www.oecd-ilibrary.org/energy/global-ev-outlook-2019_35fb60bd-en (accessed on 20 June 2019).
33. Burchartkorol, D.; Jursova, S.; Folęga, P.; Korol, J.; Pustejovska, P.; Blaut, A. Environmental life cycle assessment of electric vehicles in Poland and the Czech Republic. *J. Clean. Prod.* **2018**, *202*, 476–487. [CrossRef]
34. Petrauskienė, K.; Skvarnavičiūtė, M.; Dvarionienė, J. Comparative environmental life cycle assessment of electric and conventional vehicles in Lithuania. *J. Clean. Prod.* **2020**, *246*, 119042. [CrossRef]
35. Wang, M.; Wang, Y.; Chen, L.; Yang, Y.; Li, X. Carbon emission of energy consumption of the electric vehicle development scenario. *Environ. Sci. Pollut. Res.* **2021**, *28*, 42401–42413. [CrossRef] [PubMed]
36. Yang, L. Life cycle environmental assessment of electric and internal combustion engine vehicles in China. *J. Clean. Prod.* **2021**, *285*, 124899. [CrossRef]
37. Böhm, M.; Nanni, M.; Pappalardo, L. Gross polluters and vehicle emissions reduction. *Nat. Sustain.* **2022**, *5*, 699–707. [CrossRef]